

---

## Recent advances in measurement of the water vapour continuum in the far-infrared spectral region

Paul D. Green, Stuart M. Newman, Ralph J. Beeby, Jonathan E. Murray, Juliet C. Pickering and John E. Harries

*Phil. Trans. R. Soc. A* 2012 **370**, doi: 10.1098/rsta.2011.0263, published 30 April 2012

---

### Supplementary data

["Audio supplement"](#)

<http://rsta.royalsocietypublishing.org/content/suppl/2012/05/01/rsta.2011.0263.DC1.html>

### References

[This article cites 33 articles](#)

<http://rsta.royalsocietypublishing.org/content/370/1968/2637.full.html#ref-list-1>

### Subject collections

Articles on similar topics can be found in the following collections

[spectroscopy](#) (42 articles)

### Email alerting service

Receive free email alerts when new articles cite this article - sign up in the box at the top right-hand corner of the article or click [here](#)

# Recent advances in measurement of the water vapour continuum in the far-infrared spectral region

BY PAUL D. GREEN<sup>1,\*</sup>, STUART M. NEWMAN<sup>2</sup>, RALPH J. BEEBY<sup>1</sup>,  
JONATHAN E. MURRAY<sup>1</sup>, JULIET C. PICKERING<sup>1</sup> AND JOHN E. HARRIES<sup>1</sup>

<sup>1</sup>*Space and Atmospheric Physics, Blackett Laboratory, Imperial College,  
Prince Consort Road, London SW7 2BZ, UK*

<sup>2</sup>*UK Met Office, FitzRoy Road, Exeter, Devon EX1 3PB, UK*

We present a new derivation of the foreign-broadened water vapour continuum in the far-infrared (far-IR) pure rotation band between 24  $\mu\text{m}$  and 120  $\mu\text{m}$  ( $85\text{--}420\text{ cm}^{-1}$ ) from field data collected in flight campaigns of the Continuum Absorption by Visible and IR radiation and Atmospheric Relevance (CAVIAR) project with Imperial College's Tropospheric Airborne Fourier Transform Spectrometer (TAFTS) far-IR spectroradiometer instrument onboard the Facility for Airborne Atmospheric Measurement (FAAM) BAe-146 research aircraft; and compare this new derivation with those recently published in the literature in this spectral band. This new dataset validates the current Mlawer–Tobin–Clough–Kneizys–Davies (MT-CKD) 2.5 model parametrization above  $300\text{ cm}^{-1}$ , but indicates the need to strengthen the parametrization below  $300\text{ cm}^{-1}$ , by up to 50 per cent at  $100\text{ cm}^{-1}$ . Data recorded at a number of flight altitudes have allowed measurements within a wide range of column water vapour environments, greatly increasing the sensitivity of this analysis to the continuum strength.

**Keywords:** far-infrared; spectroscopy; water vapour continuum; airborne measurements

## 1. Introduction

Water vapour is the most important radiatively active gas in the Earth's atmosphere [1], with absorption bands throughout the microwave, infrared (IR) and visible spectral regions. One of these key regions is the far-IR pure rotation band (below  $600\text{ cm}^{-1}$ ) [2,3]. Modelling studies of the spectral-altitude dependence of the greenhouse effect and the atmospheric cooling rate have demonstrated that the far-IR water vapour pure rotation band is dominant in mid- and upper-tropospheric radiative cooling to space [4,5]; indeed, between 30 and 45 per cent of the outgoing longwave radiation (OLR) originates in this far-IR spectral band. With its sensitivity to upper-tropospheric water vapour, interest in this spectral region is growing within the scientific community, as it provides

\*Author for correspondence ([p.green@imperial.ac.uk](mailto:p.green@imperial.ac.uk)).

One contribution of 17 to a Theo Murphy Meeting Issue 'Water in the gas phase'.

the best accessibility for monitoring changes in upper-tropospheric humidity as a consequence of a changing climate [5,6].

Water vapour absorption in the atmosphere is typically modelled with two components, the monomer line absorption, as described by databases such as HIgh resolution TRANsmission (HITRAN) [7], and a slowly varying underlying absorption known as the continuum. The empirical Clough–Kneizys–Davies (CKD) continuum model was initially conceived to reconcile the modelled spectrum with observations [8]. Since its inception, the continuum has been updated with new observational evidence as it has become available, but these observations have been piecemeal, with significant sections of the IR water vapour spectrum either poorly measured or not measured at all. The Mlawer–Tobin CKD (MT-CKD) continuum parametrization employs ‘line-like’ tunable parameters that account for the super-Lorentzian behaviour observed near line centres and sub-Lorentzian behaviour in the far wings, which anchor the parametrization to the monomer line structure allowing some constraint when extrapolating across bands with insufficient measurements [9]; however, there is no universally accepted underlying physical model for the source of the continuum absorption.

The water vapour continuum in the far-IR contributes significant absorption in the Earth’s atmosphere, so influencing the energy fluxes that govern the greenhouse effect, effectively filling in the absorption between the monomer lines to such an extent that the lower troposphere is opaque to ground-based measurements from most locations on the planet [10]. Only at arctic and high-altitude sites does some of this spectral region become accessible from the ground.

Early work on the water vapour continuum by Bignell *et al.* [11], Bignell [12] and references therein was followed by significant laboratory measurements by Burch *et al.* [13]. More recently, the strength of the far-IR water vapour continuum was better constrained from field measurements taken during the Surface Heat Budget of the Arctic Ocean (SHEBA) project [14] with the Atmospheric Emitted Radiance Instrument (AERI) above  $400\text{ cm}^{-1}$ , reducing the far-IR CKD model parametrization at the time by 66 per cent. In the past 5 years, further ground-based campaigns have taken place to address the lack of far-IR observations, Earth Cooling by Water Vapour Radiation (ECOWAR) in Italy [15] and the Radiative Heating in Underexplored Bands Campaign (RHUBC) projects based in the Alaskan arctic and the Atacama desert [16,17]. However, published measurements from these campaigns alongside those of Green [18] do not cover the full far-IR region at one instance, nor were they able to measure the far-IR over a wide range of integrated column precipitable water vapour (PWV) amounts to explore the full width of the spectral region at its maximum sensitivity to the continuum contribution.

The Continuum Absorption by Visible and Infrared radiation and its Atmospheric Relevance (CAVIAR) project aimed to better describe the continuum with a coherent programme of laboratory and field measurements throughout the IR and visible spectrum, together with quantum-mechanical modelling, to critically assess the competing physical mechanisms for the continuum postulated within the community [19,20].

This study reports a derivation of the far-IR water vapour continuum from radiance spectra recorded during an airborne field measurement campaign. In this study, §2 describes the campaign details; §3 describes the methodology

employed, including the line-by-line radiative-transfer model and composite profile construction; §4 compares the observations and simulated radiance, and the study is concluded with §5, a discussion of the new derivation of the far-IR foreign-broadened water vapour continuum between 85 and 420 cm<sup>-1</sup>, and a comparison with other published measurements in the literature.

## 2. Field campaign description

The radiative closure study has been increasingly used over the past decade or so to assess a number of aspects of interest in remote sensing [21]. By combining spectrally resolved radiance measurements with independent measurements of the temperature and radiatively active gas profiles through the observed column, it is possible to assess the quality of the atmospheric profile measurement, spectroscopic model and databases used in the forward model, as well as the performance and calibration accuracy of the measurement instrumentation. In a well-designed experiment, all three of these objectives can be addressed simultaneously. The CAVIAR field campaigns were designed to provide these independent datasets; radiance measurements and the atmospheric state parameters in two different prevailing meteorological conditions from the UK Facility for Airborne Atmospheric Measurements (FAAM) airborne platform. The first, based over Camborne, UK in August and September 2008 provided relatively warm, moist conditions in a maritime environment, allowing sampling of the entire troposphere. The second campaign was based over the Jungfraujoch research station in the Swiss Alps in July and August 2009, providing drier, colder conditions. This study reports on data recorded during the Swiss component of the project.

### (a) Instrumentation

The *in situ* high-resolution radiance spectra were provided by the radiometers on board FAAM: the mid-IR Airborne Research Interferometer Evaluation System (ARIES) and Tropospheric Airborne Fourier Transform Spectrometer (TAFTS). ARIES is a mid-IR Michelson-style FTS with a spectral range of 550–3000 cm<sup>-1</sup> and a spectral resolution of 1.0 cm<sup>-1</sup> [22]. TAFTS operates at 80–650 cm<sup>-1</sup> at a resolution of 0.12 cm<sup>-1</sup>. The combination of the TAFTS and ARIES radiometers results in the continuous IR spectrum between 80 and 3000 cm<sup>-1</sup> being recorded. TAFTS is the only aircraft-mounted spectrally resolved far-IR instrument, so the FAAM facility is unique among aircraft platforms regarding thermal IR spectral coverage.

The atmospheric state parameters of importance in this study are temperature and humidity, and these data were available from a number of sources.

- The FAAM aircraft *in situ* probes provide profiling information from the Rosemount type 102 temperature probes, and humidity information from the general eastern (GE) (GE1011B) frost point hygrometer and the Fluorescence Water Vapour Sensor (FWVS).
- Vaisala RD93-type dropsondes released from the aircraft provide temperature and humidity profiles on descent by parachute. Typically,

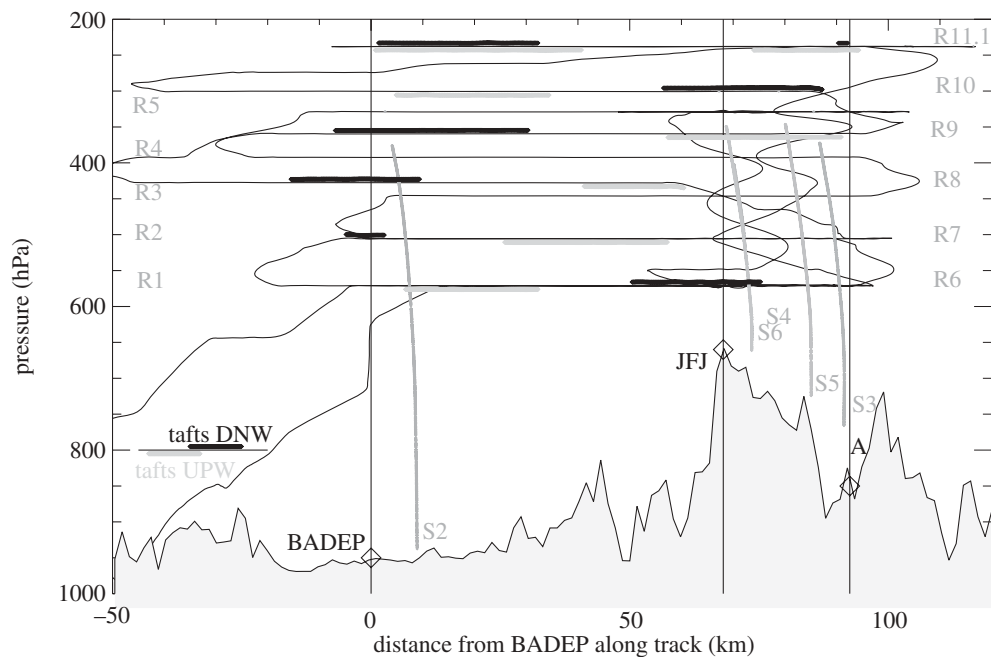


Figure 1. Projection of the runs ( $R_x$ ) from B467 onto the BADEP to A track, indicating the run segments where the upwelling (tafts UPW) and downwelling (tafts DNW) radiance data, the gaps between the sky view data segments indicate the sections of the runs spent recording calibration scans. The dropsonde launch altitudes and locations are also shown ( $S_x$ ).

six to eight were dropped from FAAM per flight from high altitude runs ( $>7925$  m).

- Vaisala RS92-type radiosonde launches from a nearby meteorological station.

(b) *The Tropospheric Airborne Fourier Transform Spectrometer instrument*

The far-IR high-spectral resolution radiances used in this study are from the Imperial College London TAFTS instrument [23,24]. TAFTS is a polarizing, Martin–Puplett-type differential interferometer [25] operating at  $80\text{--}650\text{ cm}^{-1}$  ( $16\text{--}120\text{ }\mu\text{m}$ ) at an apodized resolution of  $0.12\text{ cm}^{-1}$ , spread across two liquid-helium-cooled detector channels of  $80\text{--}300\text{ cm}^{-1}$  (Ge:Ga) and  $330\text{--}650\text{ cm}^{-1}$  (Si:Sb), known as the longwave and shortwave channels, respectively. The polarization configuration of the instrument allows both complementary outputs to be recorded in each channel, resulting in four spectra from each scan. The differential nature of the instrument allows measurement of both the upwelling and downwelling radiance incident at TAFTS, with a typical operation sequence cycling through combinations of targets that provide direct net radiance (up-downwelling), sky view against calibration blackbody and pure calibration blackbody–blackbody measurements. This cycle produces short (2 min) segments of sky view radiance data interspersed by calibration cycles. Figure 1 indicates the run segments where the upwelling and downwelling sky view segments were recorded during flight B467, with the gaps representing the time spent

performing the internal calibration scans. A single scan on TAFTS nominally takes 2 s (190 m at  $92.6 \text{ ms}^{-1}$ ), with a typical sky view cycle involving 16 scans versus a hot blackbody, then 16 versus a cold blackbody, repeated twice, giving 64 scans averaged in each analysed radiance spectrum used in this study, covering a nominal 12.2 km. TAFTS contains four calibration blackbodies, two associated with each input, one heated to 40–60°C, the other 0–25°C, designated hot and cold, respectively. Each blackbody is of an identical design, but is controlled and monitored independently. The differential design of TAFTS results in a separation of the optical path to the two inputs, so calibration blackbodies are required in both arms for accurate radiometric calibration.

The TAFTS radiometric calibration follows the algorithm of Revercomb *et al.* [26], with some additional elements particular to the Martin–Puplett layout, the polarizing beamsplitter properties, and to correct effects owing to in-flight vibrations that manifest within the application of the Brault sampling scheme [27]. Owing to the mounting angle of the Si:Sb detectors with respect to the optical axis, a channelling effect is seen in this data channel, which is also removed in post-processing. Typical random uncertainty, in radiance units (RU), for this analysis are 0.25 RU at  $80 \text{ cm}^{-1}$ , 0.2 RU at  $140 \text{ cm}^{-1}$ , rising to 0.5 RU at  $280 \text{ cm}^{-1}$  in the Ge:Ga channel, and 0.7 RU at  $330 \text{ cm}^{-1}$ , rising to 2.0 RU at  $450 \text{ cm}^{-1}$  and 5.0 RU at  $550 \text{ cm}^{-1}$  in the Si:Sb channel, where 1 RU is  $1 \text{ mW m}^{-2} \text{ sr}^{-1} (\text{cm}^{-1})^{-1}$ . These uncertainties are incorporated into the continuum determination presented herein. As part of the CAVIAR project, a purpose-built blackbody was produced by the National Physical Laboratory (Teddington, UK), traceable to internationally recognized absolute standards. Details of the TAFTS radiometric calibration are currently being prepared for publication.

TAFTS has previously flown on the UK Met Office C-130 (1998–2001) and Airborne Research Australia Egrett (2001 and 2002) before installation on the UK Natural Environment Research Council/UK Met Office FAAM aircraft in 2006 [24,28]. Green [18] detailed the first determination of the water vapour foreign-broadened continuum between 100 and  $300 \text{ cm}^{-1}$  from TAFTS data taken aboard the UK Meteorological Research Flight C-130 in 1999, however, the results from that study were limited by the lack of constraint in the atmospheric state; this study builds on the earlier work.

### 3. Methodology

The recording of radiance spectra from an airborne platform provides a number of advantages. The first has been mentioned, in that radiance measurements can be recorded at a number of altitudes, temperature and column water vapour conditions in a short period of time, within a stable atmosphere. But importantly, the aircraft platform can also sample that atmosphere, providing *in situ* and remotely sensed measurements of the temperature and humidity structure, and its evolution over the few hours of the flight in a detailed way, constraining the variability in the critical parameters to a degree difficult to achieve otherwise. This section continues with a description of the line-by-line radiative transfer model used, followed by the determination of the atmospheric profiles and their uncertainties.

*(a) The line-by-line radiative-transfer model*

For this study, the latest release of the Line-by-Line Radiative Transfer Model (LBLRTM) [9] v. 12.0 that incorporates the MT-CKD 2.5 continuum parametrization has been used. It should be noted the latest update in the far-IR continuum parameters was in v. 2.4, so v. 2.4 and v. 2.5 are identical in this spectral region. The line parameters used in LBLRTM (for v. 12.0—AER v. 3.0) are based on the latest HITRAN 2008 [7] spectroscopic database with additional updates in the far-IR principally from Gordon *et al.* [29] and Delamere *et al.* [17]. A fuller description of recent revisions in the far-IR can be found in Delamere *et al.* [17] and on the Atmospheric and Environmental Research (AER) Inc. website (<http://rtweb.aer.com>). LBLRTM is widely used as a forward model within the community and performed well in a model comparison exercise in the far-IR [30]. The model input is a profile of temperature and radiatively important gas concentrations on a pressure height scale, and allows the user to fractionally vary the strength of the continuum components employed. The profiles used in this study are on 150 fixed pressure levels, with 100 levels in the troposphere (1000–100 hPa) and 50 levels between 100 and 10 hPa; the derived profiles are interpolated onto this pressure grid.

*(b) Details of the case study flight*

The data used in this study are from flight B467 on 19 July 2009, one of nine sorties that took place in the Swiss phase of the CAVIAR flying programme. Flight B467 was chosen for this case study as good clear sky conditions persisted throughout the flight, and initial analysis of the dropsonde data showed a persistent, stable humidity structure.

Figures 1 and 2 show the flight track for flight B467 on 19 July 2009, which is typical for all the flights in the CAVIAR flight campaign. Waypoints are defined, between which flight legs were flown at a number of altitudes, in this case BADEP, A and the Jungfrauoch (JFJ) research station. A series of stepped profiles were performed, starting at the lowest altitude allowable (4877 m, 571 hPa) increasing to the maximum achievable altitude, followed by a spiral descent to the lowest allowed altitude followed by a repeat of the stepped profile to maximum altitude. At each step, a level run was performed between BADEP and point A, overpassing the JFJ station. On the higher level runs ( $\geq 7315$  m,  $\leq 400$  hPa), RD93 dropsondes were dropped from the aircraft to sample the column temperature, humidity and wind field profiles below.

Downwelling radiance spectra from five runs (numbered R6–10) are used to derive the foreign-broadened continuum. Separate atmospheric state profiles have been constructed for each run, specifically for the time and location of the radiance data combining the most relevant profile data from the instrumental data sources available, this process is described in §3c.

*(c) Determination of the atmospheric profiles*

The accurate determination of an atmospheric state profile representative of the column observed by the radiometers on board FAAM is key to this study. In the real atmosphere, the temperature and humidity vary and evolve as a function of geographical location and time, and cannot be assumed

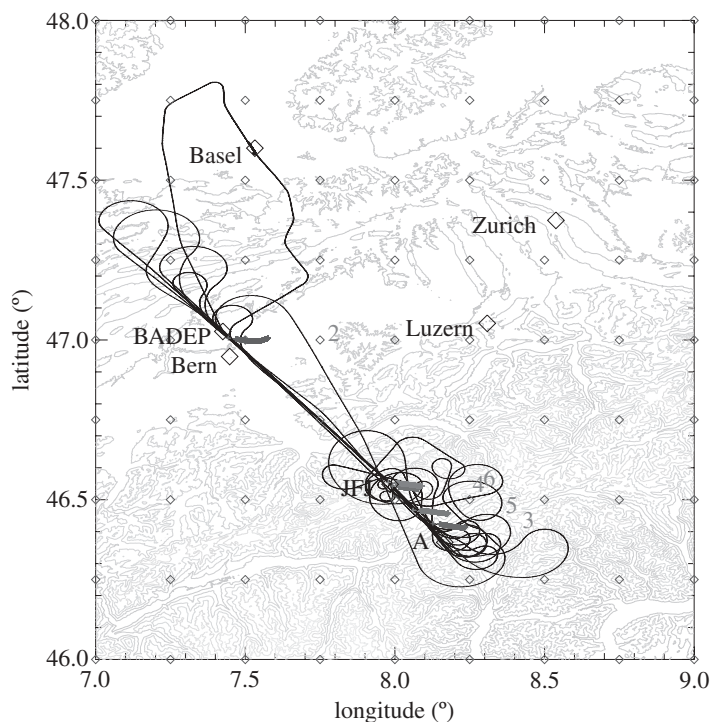


Figure 2. Map of the flight track. The flight track of B467 on 19 July 2009 is shown in black, with the flight waypoints; BADEP, A and JFC shown as diamonds. Dropsonde launches are numbered and denoted by small symbols tracking away from the flight track in an easterly direction. The European Centre for Medium-range Weather Forecasts model grid is in small diamonds at  $0.25^\circ \times 0.25^\circ$  resolution.

to remain constant. The two main quantities needed for this analysis are humidity and temperature, with humidity well known for showing high variability on short time and spatial scales. For this experiment, a number of sources of temperature and humidity data are available, and a major part of this work constituted the critical analysis of these various sources to create a composite profile that best represented the atmosphere at the required location and time.

The baseline profile was obtained from the 0Z and 12Z European Centre for Medium-range Weather Forecasts (ECMWF) analysis and 3 hourly forecast fields on a  $0.25^\circ \times 0.25^\circ$  grid, as represented by the small black diamonds in figure 2. The surface to 0.01 hPa profile is interpolated to the mean time and geographical location for the averaged radiance spectrum for each run. The ECMWF humidity and temperature fields provide profile information in the upper atmosphere above the tropopause beyond the range of *in situ* measurements and are more representative than climatology alternatives. It must be stressed that the measured far-IR radiance is not overly sensitive to the stratospheric humidity, however, vastly unrealistic values could be detrimental to the analysis. The relevant ECMWF fields for flight B467 show little variation in time for a given location.

Superimposed on the ECMWF baseline is the sonde data from the Airborne Vertical Atmospheric Profiler System (AVAPS) (<http://www.vaisala.com/en/meteorology/products/soundingsystemsandradiosondes>), and at altitudes where this is not available, Miloshevich *et al.* [31] corrected radiosonde data from the Payerne station (46.843N 6.913E) is also used. The sonde data provide both a more accurate measure for the profile during the flight than the ECMWF fields, but additionally contain much higher vertical resolution, better describing the detailed structure of the humidity and temperature fields. The Vaisala RD93 sonde has a quoted temperature accuracy of 0.1°C, with a repeatability uncertainty of 0.2°C, and humidity repeatability accuracy in relative humidity units of 2 per cent, with an overall profile uncertainty of 5 per cent. The dropsonde data were not corrected via the Miloshevich scheme, as would be applicable to ascending sondes, as factors including the greater rate of descent, air flow and dropsonde packaging design mean the RD93 sondes do not suffer from daytime solar heating to the same extent (A. Vance 2011, personal communication).

In many cases, the *in situ* aircraft data provide the most concurrent measurements to the recorded radiances. Following a stepped profile flight pattern, the profile climb/descent at each end of the run provides detailed measurements of the humidity in the region directly above and below the run level, which in many cases, as demonstrated through analysis of the analytic Jacobian product, constitutes a significant profile contribution to the measured radiance, as shown in §3*d*. After the run at maximum altitude, the aircraft profiled from maximum to minimum altitude in one phase, in a spiral descent over the JFJ station, giving an excellent profile for use in the subsequent runs. At altitudes above the dropsonde data, the *in situ* dataset is most representative. Dropsondes were typically dropped at around 300 hPa, but take some time, and therefore altitude, to register representative data. Figure 1 shows the extent of the useful data from all the sondes dropped, including those released from the run at 300 hPa. This limits the profile data to pressures above 350–400 hPa. Therefore, the *in situ* FAAM aircraft profile data have been inserted into the profile in those cases where it is more concurrent in time and space to the measured radiance spectra than the available sonde data.

The aircraft temperature measurements are recorded by two Goodrich Rosemount type 102 probes, with a time response of 1 s and uncertainty of  $\pm 0.3$  K (<http://www.faam.ac.uk>). The two humidity sensors used on the FAAM are the GE (GE1011B) frost point hygrometer and the FWVS. The GE (<http://www.faam.ac.uk>) has a dew point temperature resolution of 0.03°C and accuracy uncertainty that rises from 0.25°C at 0°C to 1.0°C at  $-60.0$ °C, whereas the response time rises from a few seconds to several minutes over the same range of ambient temperatures [32], and this is a consideration in profiles recorded at higher altitude. Despite this, the GE is a well-understood and tested instrument with excellent intrinsic accuracy. In contrast, the FWVS instrument provides a high temporal resolution dataset, with good stability but limited intrinsic accuracy. This absolute accuracy uncertainty is overcome by cross-calibration against the GE instrument. The FWVS is in development by a team at the UK Met Office who have studied the stability and reliability of the GE-based calibration from all the CAVIAR flights in 2008 and 2009, and have provided reliable calibration constants for this dataset (D. Tiddeman 2011, personal communication).

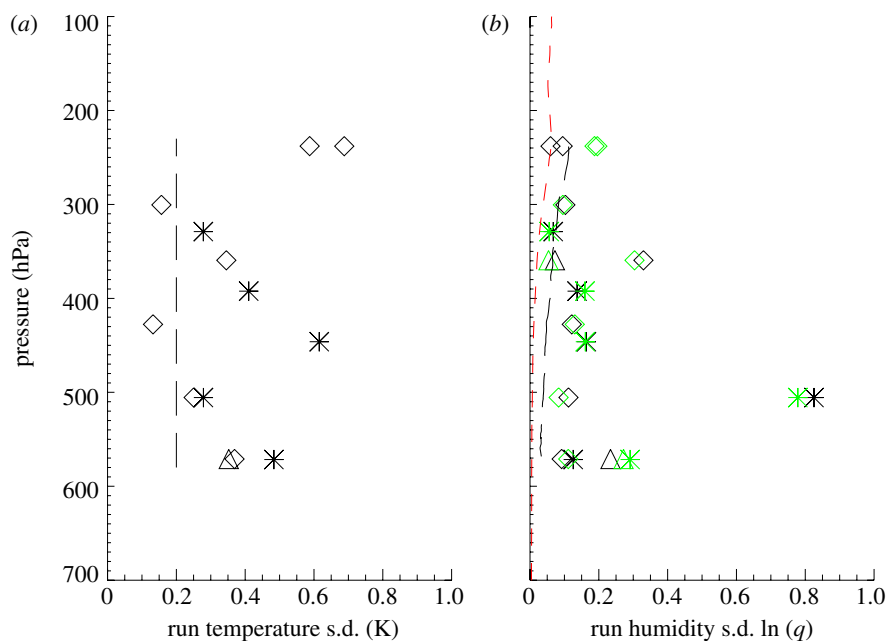


Figure 3. Profile uncertainty. (a) Along run temperature s.d. as a function of the run pressure height. The asterisks denote R1-5 (from 571 to 330 hPa), diamonds denote R6-11 (from 571 to 238 hPa), run 12 is denoted with a triangle. The vertical dashed line denotes the  $0.2^{\circ}\text{C}$  measurement uncertainty. (b) Equivalent for the humidity variability, as measured by the GE (black diamonds, triangles and asterisks) and FWVS (coloured diamonds, triangles and asterisks) instruments. The long dashed line (aircraft) represents a typical measurement uncertainty in the GE (from a spiral descent), whereas the short dashed line (sonde) denotes a 5% RH uncertainty representative of a sonde measurement. (Online version in colour.)

#### (d) Profile uncertainty

The uncertainties in the temperature and humidity profiles need to be addressed, as these are critical to the accuracy of the determination of the continuum coefficients; uncertainty in the humidity profile maps directly into uncertainty in the derived continuum. With the construction of a composite temperature and humidity profile, from a number of data sources, it is necessary to consider the composite effect of their individual uncertainties. However, two other key aspects need also be examined, the representation uncertainty and the sensitivity of the recorded radiance to the atmospheric state profile at a given distance from the aircraft.

The representation uncertainty centres on the parameter variability over the whole measurement period. This variability impacts the relevance of a measurement at a given altitude and location to the likely parameter value at that altitude when remotely viewed from a different altitude at some other time. Figure 3 shows the 1 s.d. variability of temperature and humidity measured along each run plotted at the altitude of that run, as measured by the *in situ* instruments on the FAAM aircraft. These plots are not shown to demonstrate the characteristic behaviour of the instruments in a given temperature and humidity

Table 1. The precipitable water vapour (PWV) column amount above the observation altitude for each of the five runs used in the analysis. For reference, the total column at Payerne (489 m altitude) for this period was 17–18 mm.

run no.	run pressure (hPa)	PWV (mm)	PWV uncertainty (%)
6	571.0	1.91	2.0
7	505.4	1.26	2.5
8	427.6	1.21	2.9
9	359.6	0.547	1.9
10	300.6	0.195	3.0

regime, but to show the relative magnitude of the variability observed along a run to that of the instrumental uncertainty, and thus explore the more significant source of uncertainty.

Considering the temperature uncertainty in figure 3*a*, the mean 1 s.d. variation over all levels is  $\pm 0.38^\circ\text{C}$  with a range from  $\pm 0.13^\circ\text{C}$  to  $\pm 0.68^\circ\text{C}$ . At almost all levels, the variability exceeds the measurement accuracy of the instruments. A point measurement may be more accurate, but would not convey the variability that exists in the atmosphere. The measurement accuracy, however, is a lower limit to the absolute knowledge in the temperature, so for uncertainty analysis purposes at the pressure levels where the variability falls below the measurement accuracy of  $\pm 0.2^\circ\text{C}$ , the uncertainty has been set to this level.

The humidity data are shown in figure 3*b* for the two aircraft sensors. In all but the highest altitude run, the GE and FWVS variability show good agreement. At the highest level, the FWVS variability exceeds that of the GE and is a consequence of the GE lengthening time response in cold conditions. The two dashed lines represent the measurement uncertainty in the GE and sonde. The variability observed at all altitude levels exceeds the sonde measurement uncertainty, and is equal to or greater than the GE accuracy. At low altitude, the variability along the run far exceeds the measurement uncertainty. Run 2 at 505 hPa is exceptional, and is a consequence of a different, drier airmass being present at the northwestern end of the run at that time and altitude. Radiance data are not analysed from runs 1 to 5, so this run 2 variability measurement is not included in the derived profile uncertainty. The variability measurements are taken over a period of at maximum 10 min, along a 100 km track, indicating that variability exists on a small scale. This variability governs the maximum accuracy that the humidity can be effectively represented when creating the simulated radiances, even though a sonde profile, for instance, is capable of making a point measurement with greater accuracy. For this reason, the s.d. of the variability along each run will be used as the humidity uncertainty at that altitude, and points between run levels will be interpolated between run levels to preserve the vertical structure of the variability. Where the GE and FWVS variability do not agree, the FWVS values are used, as the faster instrument time response indicates this as a more accurate estimate of the variability. Table 1 shows how this variability analysis translates to the uncertainty in the total column PWV for each observation run, treated as an uncorrelated uncertainty with respect to altitude alongside the PWV column value for that run.

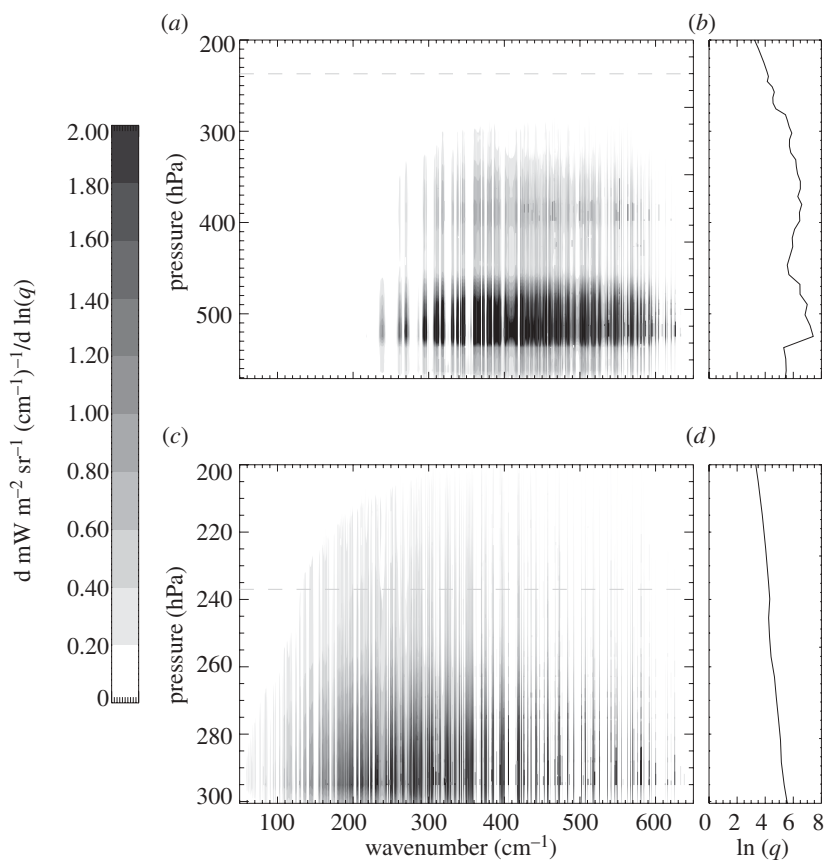


Figure 4. Analytic Jacobian simulation with respect to humidity,  $q$ , for the downwelling radiance recorded on run 6 at 571 hPa (a) and run 10 at 300 hPa (c). (b,d) The corresponding humidity profiles for (a,c). The dashed line at 237 hPa indicates the maximum extent of the aircraft *in situ* measurements.

The second point to consider regarding profile uncertainty is the sensitivity of the radiance to the profile structure along the line of sight. Analytic Jacobian analysis is useful in this work, as it indicates the sections of the profile that most contribute to the radiance at the flight level, and importantly those parts of the profile that the recorded radiance is insensitive to. The algorithm behind the analytic Jacobian will not be discussed here, although put simply, it represents the sensitivity of the radiance at a given pressure level to a unit change in absorber amount (or temperature) in the viewed profile.

Figure 4 shows the analytic Jacobian with respect to humidity for the simulated downwelling radiance for the lowest and highest altitude run used in this analysis. For run 6, figure 4a, the majority of the sensitivity in the microwindows between 300 and 600  $\text{cm}^{-1}$  is between 540 and 460 hPa, with some reduced sensitivity up to 300 hPa. Given that the far-IR radiance has very little sensitivity to the profile above 300 hPa for this run, an accurate knowledge of the profile at higher altitudes is unnecessary, relaxing the constraint needed on the profile and its uncertainty.

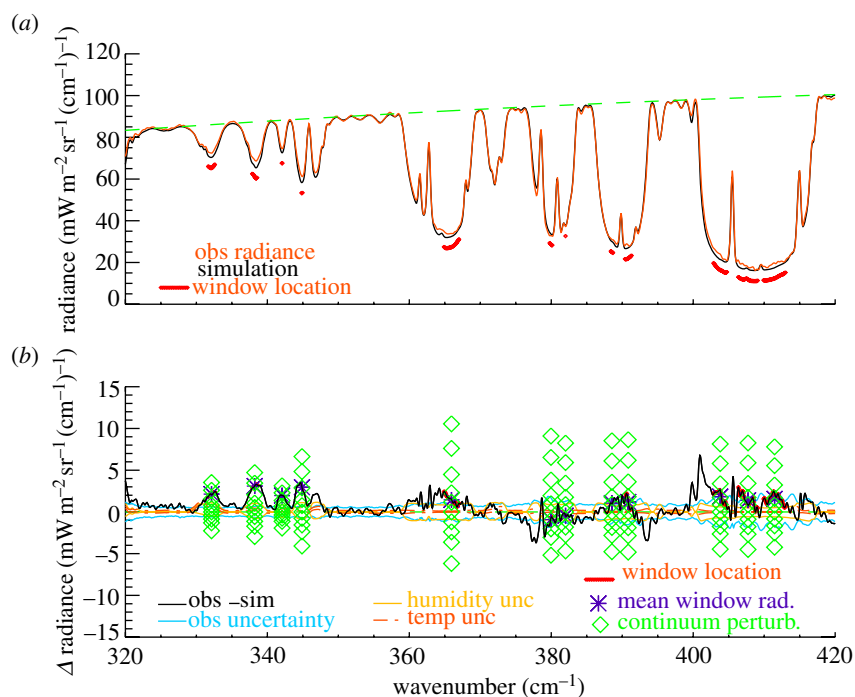


Figure 5. Comparison of the TAFTS and simulated radiances. (a) Section of the TAFTS data, with the corresponding simulated radiance. (b) Denotes the observation – simulation residual in black. The TAFTS radiometric calibration uncertainty level, profile uncertainty in terms of temperature and humidity are also plotted. The continuum sensitivity calculations are denoted by diamonds from 50 to 200% variation. (Online version in colour.)

Figure 4c shows the same Jacobian analysis for the highest run at 300 hPa; even here, the majority of the radiance sensitivity, below  $350 \text{ cm}^{-1}$ , is within the range of the aircraft *in situ* measurements at pressures down to 237 hPa, and therefore well constrained. Downwelling radiance data from run 11 at 237 hPa have not been used in this analysis because of the uncertainty in the overlying profile outside the reach of the *in situ* measurements.

## 4. Results

### (a) Simulation–observation comparison

Simulated radiances are compared with the calibrated TAFTS spectra for each of the five downwelling views between 571 and 300 hPa recorded on runs 6–10. Figure 5 shows a typical comparison for a subset of the TAFTS downwelling data at 571 hPa between 320 and  $420 \text{ cm}^{-1}$ . Figure 5a shows the TAFTS radiance and simulation. The dashed line is a Planck curve at the mean local air temperature at the run level of 265.0 K. The extent of each window is highlighted by the solid band below the radiance spectrum. For each window comparison, the average of all spectral points within this designated window zone is used (both in the

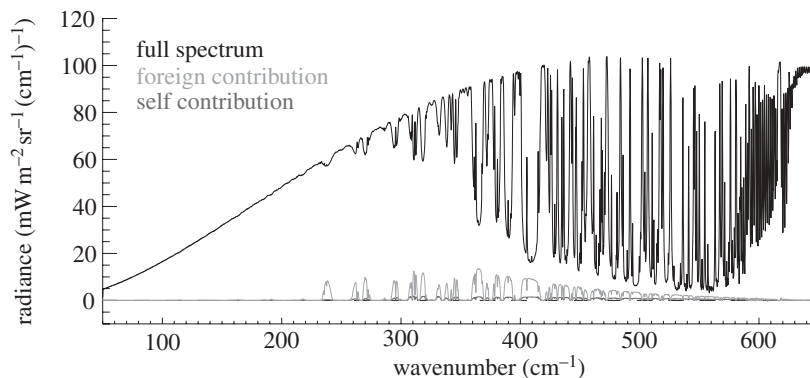


Figure 6. The modelled contribution to the downwelling radiance spectrum of the foreign-broadened and self-broadened continuum for run 6 at 571 hPa. The relevant profile is shown in figure 4*b*.

measured and simulated spectra). The extent of the window zone is determined from a maximum local gradient criteria around the window minimum in the radiance spectrum. Figure 5*b* indicates the difference observation – simulation for the same spectral region. Additionally, plotted here is the radiometric calibration uncertainty in the TAFTS data, specific to the data used for this run and the radiance equivalent uncertainty in the temperature and humidity profile. Microwindows are denoted as sections of small diamond symbols on the radiance difference. It should be noted that the number of microwindows varies with altitude, with additional windows opening up with increasing altitude. The asterisks indicate the mean radiance difference within the microwindow, and the diamonds show the equivalent net radiance difference for a change in water vapour foreign continuum strength between factors of 0.5 and 2.0 from MT-CKD 2.5. The net radiance window differences are fitted to these simulated perturbed continuum values, to determine the necessary alteration to the continuum parametrization. The foreign-broadened continuum is the dominant contribution in this spectral region, as seen in figure 6, although the self-broadened component is not completely negligible at 571 hPa, modelling suggests the self-broadened contribution is 5–10 times lower than the foreign-broadened contribution in the major windows, and well below the radiometric calibration limit of the radiance spectra. At increasing run altitudes, the self-broadened contribution falls rapidly, with the foreign: self contribution ratio greater than 100:1 at 300 hPa in the spectral region with greatest continuum sensitivity. As it is not possible to separate the contributions from the observed radiance spectra or profile information, the model is relied on in this aspect, and all net radiance differences are attributed to the foreign-broadened component.

Figure 7 shows the results of the derived continuum strength across the TAFTS spectral range compared with that in MT-CKD 2.5 as employed in LBLRTM v. 12.0. To ensure that only microwindows with sufficient sensitivity to the continuum are used at each flight level, a selection criterion has been applied, whereby the radiance uncertainty is equated to its effective continuum perturbation, and windows are included only if the uncertainty falls below a given threshold. This threshold was chosen as a radiance equivalent continuum

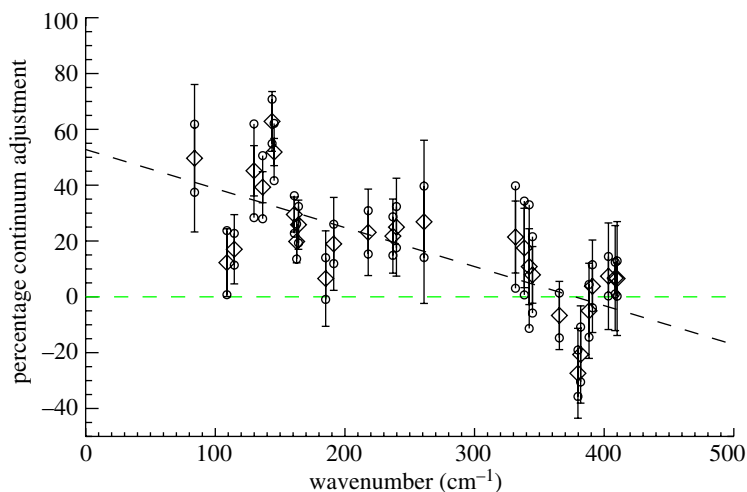


Figure 7. Derived continuum perturbations from the current model, MT-CKD 2.5. The horizontal error bar terminators are the equivalent continuum perturbation of the TAFTS radiance uncertainty, the circle terminator error bars are equivalent to the profile error. These uncertainties are combined in the analysis, but separated here to indicate the relative importance of the two main uncertainty sources. (Online version in colour.)

perturbation of 30 per cent; however, a sensitivity study into the choice of threshold demonstrated a robust result over a range of threshold values. The derived continuum perturbation from each run altitude is then averaged for each window. The horizontal error bar terminators represent the change in continuum equivalent to the TAFTS radiance uncertainty level, and profile uncertainty is represented by circle terminators for each window, respectively. The profile uncertainty in the majority of windows is about one-half that of the radiometric uncertainty in the TAFTS spectra. Table 2 contains the newly derived foreign-broadened continuum spectral density function parameters for each of the microwindows, with their associated combined uncertainties as plotted in figure 7.

## 5. Discussion

We present new measurements of the water vapour foreign-broadened continuum in the far-IR  $85\text{--}420\text{ cm}^{-1}$  spectral region recorded during the flight campaign phase of the CAVIAR consortium project. These are the first continuum coefficients published in the  $85\text{--}240\text{ cm}^{-1}$  region and the first to span the entire pure rotation band in one measurement campaign. Figure 8 shows these results in context with respect to the recent evolution of the continuum parametrization used in line-by-line models and other work on the water vapour continuum in the far-IR. Compared with the most recent evolution of the MT-CKD parametrization, this study indicates agreement within uncertainties above  $300\text{ cm}^{-1}$ , and a stronger continuum through the centre of the far-IR region below

Table 2. The derived foreign-broadened spectral density function values for each microwindow alongside the associated uncertainty as derived in this study.  $C_f \times 10^{-24}$  ( $\text{cm}^{-1} \text{mol cm}^{-2}$ ) $^{-1}$ .

wavenumber ( $\text{cm}^{-1}$ )	continuum strength $C_f \times 10^{-24}$	uncertainty $C_f \times 10^{-24}$	uncertainty (%)
84.0	169	32	19.4
109.0	96.8	14.4	14.9
114.7	93.5	10.9	11.6
129.9	92.0	12.0	13.1
136.5	79.2	7.2	9.0
143.8	82.3	6.7	8.2
145.4	74.8	5.6	7.5
161.0	48.5	3.4	7.1
162.8	43.4	3.6	8.2
164.2	44.4	3.9	8.7
185.1	24.8	4.3	17.5
191.4	24.0	3.7	15.2
218.0	14.0	2.0	14.1
237.0	8.95	1.10	12.3
239.7	8.45	1.29	15.2
261.0	4.98	1.25	25.1
331.6	1.06	0.20	18.5
338.4	0.889	0.167	18.7
342.1	0.783	0.184	23.5
344.7	0.733	0.116	15.8
365.4	0.431	0.068	15.7
379.8	0.259	0.065	25.0
381.8	0.272	0.069	25.2
388.3	0.282	0.058	20.5
390.9	0.291	0.051	17.6
403.3	0.244	0.046	19.0
408.5	0.220	0.040	18.4
410.0	0.213	0.043	20.0

$300 \text{ cm}^{-1}$ , showing better agreement with the earlier MT-CKD 1.0/2.0 parameters at  $100 \text{ cm}^{-1}$ , thus indicating that the reduction seen in the latest evolution, v. 2.5, is too severe in the  $80\text{--}300 \text{ cm}^{-1}$  spectral region.

With respect to recent measurements, these newly derived continuum coefficients compare within uncertainties, with the work of Serio *et al.* [15] and the RHUBC measurements above  $400 \text{ cm}^{-1}$  by Delamere *et al.* [17]. The initial results below  $200 \text{ cm}^{-1}$  from Green [18] also show agreement, within uncertainties, with this study, although the two Green [18] points above  $200 \text{ cm}^{-1}$  in that study do suggest a greater continuum strength between  $200$  and  $250 \text{ cm}^{-1}$  than Serio *et al.* [15] and this study.

Figure 9 shows the implication of the new parametrization on the clear sky OLR in a subarctic winter standard atmosphere. Figure 9a denotes the fluxes as calculated using the MT-CKD 2.5 water vapour foreign-broadened parameters, whereas figure 9b denotes the change to the fluxes with the new parameters presented here. With an increase in the continuum coefficients, the atmospheric

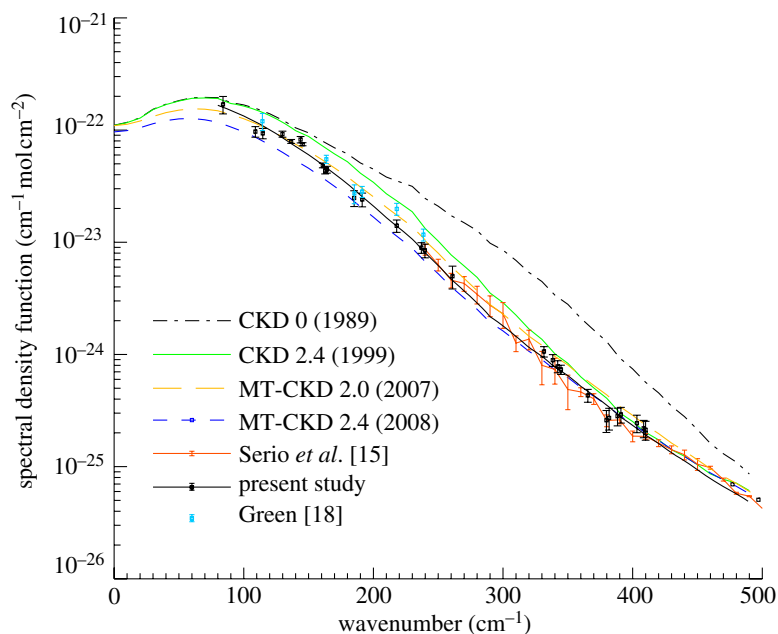


Figure 8. The continuum perturbation results from this study compared with the evolution of the MT-CKD model and recent published results from the literature. (Online version in colour.)

opacity in this spectral region is increased in the mid- to upper troposphere, increasing the downwelling flux, with a maximum increase of  $+0.19 \text{ W m}^{-2}$  at 450 hPa. The increase in opacity shifts the mean upwelling flux emission pressure higher in the troposphere, reducing the mean emission temperature and correspondingly, reducing the upwelling flux at the tropopause by  $-0.04 \text{ W m}^{-2}$ .

The far-IR monomer line parameter uncertainty has not been addressed in this work. The AER v. 3.0 line list used does incorporate updates in the far-IR, as presented in Delamere *et al.* [17]. Uncertainties in the line strengths, positions and widths may have some influence on the results; however, only the centres of the microwindows were considered, reducing the influence of this uncertainty. TAFTS radiance data are of higher spectral resolution ( $0.12 \text{ cm}^{-1}$ ) than many of its contemporary instruments, Far-Infrared Spectroscopy of the Troposphere (FIRST) [33], Radiation Explorer in the Far Infrared (REFIR) [34] and the AERI extended range [35] (typically around  $0.5 \text{ cm}^{-1}$ ), and the CAVIAR dataset would be an excellent opportunity to test the monomer spectroscopy in this spectral region. The CAVIAR dataset could be exploited further to validate the separation between the self- and foreign-broadened continuum, as well as explore any temperature dependence that may exist, given the range of PWV amounts and temperature regimes accessible from aircraft measurements throughout the troposphere.

The data used in this study are from just one of the 10 flights that took place in the CAVIAR campaign, and further analysis of this valuable dataset would reduce the uncertainties on the continuum parametrization presented. Equivalent analysis for flight B400 over Camborne on 18 September 2008 is progressing well, and will be published soon [36].

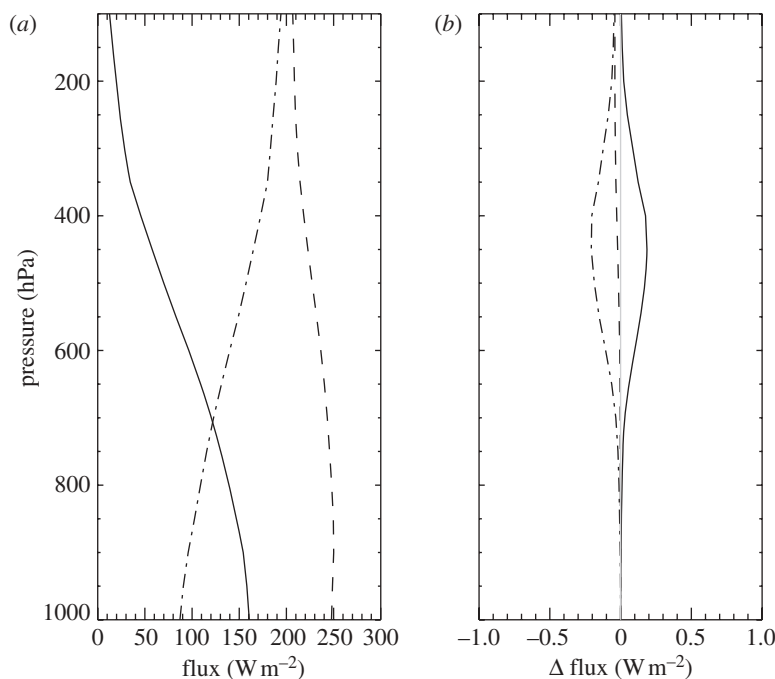


Figure 9. Impact of the newly derived continuum parameters on the clear sky longwave fluxes ( $50\text{--}2500\text{ cm}^{-1}$ ) in a subarctic winter standard atmosphere. (a) Total IR upwelling (long dashed line), downwelling (solid line) and net tropospheric fluxes (small dashed line). (b) The change to the fluxes with the water vapour foreign-broadened continuum increase below  $380\text{ cm}^{-1}$  in accordance with the results presented in this study.

The analysis and continuum measurement results presented here have highlighted the strict constraints on the atmospheric profile and radiometric accuracy of the radiance measurements needed to adequately constrain the pure rotation band foreign continuum. An accurate representation of the continuum is needed to determine the atmospheric fluxes that govern the planet's radiative cooling mechanism. With predicted changes to upper tropospheric humidity as a consequence of a changing climate, an accurate understanding on how the humidity perturbation will affect the fluxes is key. Additionally, with satellite missions proposed to monitor the far-IR spectrum from space, accurate spectroscopy in this region is necessary to fully use the datasets created.

This work is funded under the NERC CAVIAR consortium (grant no. NE/D010764/1). The authors thank Alan Last at Imperial College for his work with the TAFTS instrument development; Liam Tallis at Reading University for the ECMWF data; Tom Gardiner, Marc Coleman and Eric Usadi at the National Physical Laboratory for their participation in the calibration exercises; Dave Tiddeman, Alan Vance and Debbie O'Sullivan at the UK Met Office for data and useful discussion on the aircraft humidity measurements; and Keith Shine for his tireless leadership of the CAVIAR consortium. FAAM is jointly funded by the Met Office and the Natural Environment Research Council. We thank the staff at FAAM, DirectFlight Ltd and Avalon Aero Ltd. for their efforts throughout the flight campaigns.

## References

- 1 Harries, J. E. 1996 The greenhouse Earth: a view from space. *Q. J. R. Meteorol. Soc.* **122**, 799–818. (doi:10.1002/qj.49712253202)
- 2 Clough, S. A., Iacono, M. J. & Moncet, J. L. 1992 Line by line calculations of atmospheric fluxes and cooling rates: application to water vapor. *J. Geophys. Res.* **97**, 15 761–15 785. (doi:10.1029/92JD01419)
- 3 Sinha, A. & Harries, J. E. 1995 Water vapour and the greenhouse trapping: the role of far infra-red absorption. *Geophys. Res. Lett.* **22**, 2147–2150. (doi:10.1029/95GL01891)
- 4 Brindley, H. E. & Harries, J. E. 1998 The impact of far infra-red absorption on clear sky greenhouse forcing: sensitivity studies at high spectral resolution. *J. Quant. Spectrosc. Radiat. Transf.* **60**, 151–180. (doi:10.1016/S0022-4073(97)00152-0)
- 5 Harries, J. E., Carli, B., Rizzi, R., Serio, C., Mlynchzak, M., Palchetti, L., Maestri, T., Brindley, H. & Masiello, G. 2008 The far-infrared Earth. *Rev. Geophys.* **46**, RG4004. (doi:10.1029/2007RG000233)
- 6 Shaw, J. A., Bates, J. J., Zorn, M. Z. & Churnside, J. H. 1999 Observations of the down-welling infrared spectral radiance at Mauna Loa, Hawaii during the 1997–1998 ENSO event. *Geophys. Res. Lett.* **26**, 1727–1730. (doi:10.1029/1999GL900362)
- 7 Rothman, L. S. 2009 The HITRAN 2008 molecular spectroscopic database. *J. Quant. Spectrosc. Radiat. Transf.* **110**, 533–572. (doi:10.1016/j.jqsrt.2009.02.013)
- 8 Clough, S. A., Kneizys, F. X. & Davies, R. W. 1989 Line shape and the water vapor continuum. *Atmos. Res.* **23**, 229–241. (doi:10.1016/0169-8095(89)90020-3)
- 9 Clough, S. A., Shephard, M. W., Mlawer, E. J., Delamere, J. S., Iacono, M. J., Cady-Pereira, K., Boukabara, S. & Brown, P. D. 2005 Atmospheric radiative transfer modeling: a summary of the AER codes. *J. Quant. Spectrosc. Radiat. Transf.* **91**, 233–244. (doi:10.1016/j.jqsrt.2004.05.058)
- 10 Davis, G. R. 1993 The far infrared continuum absorption of water vapour. *J. Quant. Spectrosc. Radiat. Transf.* **50**, 673–694. (doi:10.1016/0022-4073(93)90034-F)
- 11 Bignell, K. J., Saiedy, F. & Sheppard, P. A. 1963 On the atmospheric infrared continuum. *J. Opt. Soc. Am.* **53**, 466–479. (doi:10.1364/JOSA.53.000466)
- 12 Bignell, K. J. 1970 The water-vapour infra-red continuum. *Q. J. R. Meteorol. Soc.* **96**, 390–403. (doi:10.1002/qj.49709640904)
- 13 Burch, D. E., Gryvnak, D. A. & Patty, R. P. 1974 Continuum absorption by H<sub>2</sub>O between 300 and 825 cm<sup>-1</sup>. Technical report no. AFCRL-TR-74-0377, Air Force Cambridge Research Laboratory, Hanscom (AFB), MA, USA.
- 14 Tobin, D. C. *et al.* 1999 Downwelling spectral radiance observations at the SHEBA ice station from 17 to 26 microns. *J. Geophys. Res.* **104**, 2081–2092. (doi:10.1029/1998JD200057)
- 15 Serio, C. *et al.* 2008 Retrieval of foreign-broadened water vapor continuum coefficients from emitted spectral radiance in the H<sub>2</sub>O rotational band from 240 to 590 cm<sup>-1</sup>. *Opt. Express* **16**, 15 816–15 833. (doi:10.1364/OE.16.015816)
- 16 Turner, D. D. & Mlawer, E. J. 2010 The radiative heating in underexplored bands campaign. *Bull. Am. Meteorol. Soc.* **91**, 911–923. (doi:10.1175/2010BAMS2904.1)
- 17 Delamere, J. S., Clough, S. A., Payne, V. H., Mlawer, E. J., Turner, D. D. & Gamache, R. R. 2010 A far-infrared radiative closure study in the Arctic: application to water vapor. *J. Geophys. Res.* **115**, D17106. (doi:10.1029/2009JD012968)
- 18 Green, P. D. 2003 The development of a fourier transform spectrometer to measure far IR fluxes in the upper troposphere. PhD thesis, University of London, UK.
- 19 Ma, Q. & Tipping, R. H. 2002 The frequency detuning correction and the asymmetry of line shapes: the far wing of H<sub>2</sub>O–H<sub>2</sub>O. *J. Chem. Phys.* **116**, 4102–4115. (doi:10.1063/1.1436115)
- 20 Ptashnik, I. V., Smith, K. M., Shine, K. P. & Newnham, D. A. 2004 Laboratory measurements of water vapor continuum absorption in spectral region 5000–5600 cm<sup>-1</sup>: evidence for water dimers. *Q. J. R. Meteorol. Soc.* **130**, 2391–2408. (doi:10.1256/qj.03.178)
- 21 Turner, D. D. *et al.* 2004 The QME AERI LBLRTM: a closure experiment for downwelling high spectral resolution infrared radiance. *J. Atmos. Sci.* **61**, 2657–2675. (doi:10.1175/JAS3300.1)
- 22 Wilson, S. H. S., Atkinson, N. C. & Smith, J. A. 1999 The development of an airborne infrared interferometer for meteorological sounding studies. *J. Atmos. Oceanic Technol.* **16**, 1912–1927. (doi:10.1175/1520-0426(1999)016<1912:TDOAAI>2.0.CO;2)

- 23 Cañas, A. A. D., Murray, J. E. & Harries, J. E. 1997 Tropospheric airborne fourier transform spectrometer (TAFTS). *SPIE* **3220**, 91–102. (doi:10.1117/12.301139)
- 24 Cox, C. V., Murray, J. E., Taylor, J. P., Green, P. D., Pickering, J. C., Harries, J. E. & Last, A. E. 2007 Clear-sky far infra-red measurements observed during the EAQUATE campaign, September 2004. *Q. J. R. Meteorol. Soc.* **133**, 273–283. (doi:10.1002/qj.159)
- 25 Martin, D. H. & Puppelt, E. 1969 Polarisation interferometric spectrometer for millimeter and submillimeter spectroscopy. *Infrared Phys.* **10**, 105–109. (doi:10.1016/0020-0891(70)90006-0)
- 26 Revercomb, H. E., Buijs, H., Howell, H. B., LaPorte, D. D., Smith, W. L. & Sromovsky, L. A. 1988 Radiometric calibration of IR Fourier transform spectrometers: solution to a problem with the high-resolution interferometer sounder. *Appl. Opt.* **27**, 3210–3218. (doi:10.1364/AO.27.003210)
- 27 Brault, J. W. 1996 New approach to high-precision Fourier transform spectrometer design. *Appl. Opt.* **35**, 2891–2896. (doi:10.1364/AO.35.002891)
- 28 Cox, C. V., Harries, J. E., Taylor, J. P., Baran, A., Green, P. D., Pickering, J. C., Murray, J. E. & Last, A. E. 2010 Measurement and simulation of mid and far infrared spectra in the presence of cirrus. *Q. J. R. Meteorol. Soc.* **136**, 718–739. (doi:10.1002/qj.596)
- 29 Gordon, I., Rothman, L., Gamache, R., Jacquemart, D., Boone, C., Bernath, P., Shephard, M., Delamere, J. & Clough, S. 2007 Current updates of the water-vapor line list in HITRAN: a new ‘diet’ for air-broadened halfwidths. *J. Quant. Spectrosc. Radiat. Transf.* **108**, 389–402. (doi:10.1016/j.jqsrt.2007.06.009)
- 30 Kratz, D., Mlynczak, M., Mertens, C., Brindley, H., Gordley, L., Martin-Torres, J., Miskolczi, F. & Turner, D. 2005 An inter-comparison of far-infrared line-by-line radiative transfer models. *J. Quant. Spectrosc. Radiat. Transf.* **90**, 323–341. (doi:10.1016/j.jqsrt.2004.04.006)
- 31 Miloshevich, L., Vomel, H., Whiteman, D. & Leblanc, T. 2009 Accuracy assessment and correction of Vaisala RS92 radiosonde water vapor measurements. *J. Geophys. Res.* **114**, D11305. (doi:10.1029/2008JD011565)
- 32 Mastenbrook, H. J. 1968 Water vapor distribution in the stratosphere and high troposphere. *J. Atmos. Sci.* **25**, 299–311. (doi:10.1175/1520-0469(1968)025<0299:WVDITS>2.0.CO;2)
- 33 Mlynczak, M. G. *et al.* 2006 First light from the far-infrared spectroscopy of the troposphere (FIRST) instrument. *Geophys. Res. Lett.* **33**, L07704. (doi:10.1029/2005GL025114)
- 34 Palchetti, L., Bianchini, G., Castagnoli, F., Carli, B., Serio, C., Esposito, F., Cuomo, V., Rizzi, R. & Maestri, T. 2005 Breadboard of the Fourier transform spectrometer for the radiation explorer in the far infrared (REFIR) atmospheric mission. *Appl. Opt.* **44**, 2870–2878. (doi:10.1364/AO.44.002870)
- 35 Knuteson, R. O. *et al.* 2004 The atmospheric emitted radiance interferometer. Part I: instrument design. *J. Atmos. Oceanic Technol.* **21**, 1763–1776. (doi:10.1175/JTECH-1662.1)
- 36 Beeby, R. In press. Validation of the far-infrared foreign-broadened water vapour continuum from airborne field campaign measurements. PhD thesis, Imperial College London, UK.